ELSEVIER J. Non-Newtonian Fluid Mech., 56 (1995) 183–216

Journal of Non-Newtonian Fluid Mechanics

Entry flow of fiber suspensions in a straight channel

Lan Tang, M. Cengiz Altan

School of Aerospace and Mechanical Engineering, University of Oklahoma, Norman, OK 73019 USA

Received 10 August 1993; in revised form 26 July 1994

Abstract

The planar channel entry flow of a Newtown fluid containing neutrally buoyant, non-Brownian, slender particles is studied numerically. In particular, the effects of Reynolds number, *Re*, and a nondimensional suspension parameter, *C*, on the developing velocity and orientation fields are investigated. The governing orientation equations are solved along particle paths, whereas the flow kinematics is determined from an Eulerian viewpoint. The fourth-order orientation tensor, which characterizes the orientation structure, is obtained from the differential orientation evolution equations and also from the Lagrangian description of the orientation angles of a number of fictitious fibers in the orientation space. It is found that both the second- and fourth-order orientation evolution equations, if used with quadratic closure approximations, inaccurately predict an earlier alignment of fibers in the flow direction. Furthermore, for higher values of suspension parameter *C*, convergent results are not obtained by using such evolution equations. On the other hand, the results obtained by following a number of orientation angles indicate that the entry length increases linearly with *C*, and the effect of Reynolds number on the entry length becomes negligible for high *C* values.

Keywords: Entry flow; Fiber suspensions; Straight channel; Suspension parameter

1. Introduction

The laminar entry flow of both Newtonian and non-Newtonian fluids has attracted considerable interest for several decades due to its technological importance in numerous applications. Most of the studies for Newtonian fluids are performed by using assumptions inherent in the boundary layer theory (see for example, Schlichting [1] and Van Dyke [2]), or by using numerical techniques [3,4].

SSDI 0377-0257(94)01280-6

The non-Newtonian entry flows have also been studied extensively where the power-law [5,6], Bingham plastic [7], or viscoelastic [8,9] flow models are used. More recently, entry flows of Newtonian, inelastic non-Newtonian, and viscoelastic flows through a sudden contraction have been reviewed in detail by Boger [10].

In recent years, with the increase in composition materials usage, interest in the rheology and processing of fiber suspensions has increased significantly. Hence, complex flows of dilute and semi-dilute fiber suspensions have been studied numerically for a few flow configurations using the constitutive equations developed in the last three decades. Initially, Evans [11] worked on the flow of fiber suspensions through a number of simple geometries, including the start-up channel flow. Approximately a decade later, the isothermal extrusion of a fiber suspension in a Newtonian medium was analyzed by Papanastasiou and Alexandrou [12] by using a constitutive model proposed for semi-dilute suspensions [13]. Lipscomb et al. [14] performed finite element simulations for the flow of suspensions through an axisymmetric contraction by using a constitutive equation similar to those developed by Batchelor [15], Evans [16], Hinch and Leal [17,18], and Ericksen [19]. Following Lipscomb et al., Chiba et al. [20] extended the results of axisymmetric contraction flow to nonzero Reynolds numbers by a finite difference scheme. In addition, Rosenberg et al. [21], and Phan-Thien and Graham [22] presented numerical simulations for the falling ball rheometry of fiber suspensions. Altan et al. [23] studied the interaction between the fluid kinematics and the orientation field resulting from the introduction of randomly oriented fibers in a fully developed channel flow. Corner and sink flows of a suspension of rigid rods have also been investigated by Keiller and coworkers [24–26].

Most of the constitutive models used in recent numerical simulations of complex suspension flows utilize similar expressions to describe the extra stresses due to the presence of particles. In essence, the suspension microstructure is characterized by a fourth-order tensor which is defined as the fourth-order moments of an orientation distribution function. Then, depending on the particle aspect ratio and concentration regime, the fourth- and sometimes the second-order orientation tensors are employed to relate the strain rate to stress tensor. For a nonhomogeneous steady suspension flow where the velocity gradients are spatially nonuniform, the conformation of microstructure and the flow kinematics are usually specified from an Eulerian view-point. However, the orientation conformation at a point depends on the fluid deformation history. Therefore, one needs to develop computationally efficient and accurate methods to determine the orientation conformation, and a Lagrangian approach may be appropriate for the deformation dependent microstructure evolution.

In this paper, we present the numerical results of the flow and orientation fields in a channel entry flow containing slender, non-Brownian fibers. We also investigate the accuracy and efficiency of commonly used methods for solving the orientation field. In particular, the following three different solution techniques are used to determine the orientation field.

(1) The orientation evolution equation for the second-order orientation tensor with a fourth-order quadratic closure approximation is solved along the particle path for each grid point.

(2) The orientation evolution equation for the fourth-order orientation tensor with

a sixth-order quadratic closure approximation is solved along the particle path for each grid point.

(3) Orientation angles for a number of trace fibers are solved analytically along the particle path for each grid point, thus forming an orientation state which is subsequently described by a fourth-order orientation tensor.

The last method proved to be the most accurate efficient one to be used in complex suspension flows. In addition, the development of flow and orientation fields, the effect of Reynolds number, the entry length, and the pressure drop are investigated, and the results are presented as a function of the nondimensional suspension parameter C.

2. Constitutive models

Several constitutive models have been proposed to describe the bulk stress tensor for suspensions of neutrally buoyant ellipsoidal particles in a Newtonian fluid. The constitutive equations for such systems, either obtained by invoking continuum mechanics principles [19] or by using microstructural information [15,17,18], have the same form despite different starting points. In general, the total viscous stress tensor for the suspension, τ_{ij}, is taken to be the sum of the stress contributions from the Newtonian suspending fluid, τ_{ij}^{f}, and from the ellipsoidal particles, τ_{ij}^{p}. Hence, the resulting constitutive equations for the suspension of rigid, non-Brownian ellipsoids of revolutions can be expressed as

$$\begin{aligned} &\tau_{ij} = \tau_{ij}^{f} + \tau_{ij}^{p}, \\ &\tau_{ij}^{f} = \mu(u_{ij} + u_{ji}), \\ &\tau_{ij}^{p} = \mu\phi_v\{AS_{ijkl}u_{kl} + B[S_{ik}(u_{kj} + u_{jk}) + (u_{ik} + u_{ki})S_{kj}] + C(u_{ij} + u_{ji})\}, \end{aligned} \tag{1}$$

where μ is the viscosity of the suspending fluid, ϕ_v is the volume fraction of the suspended particles, u_{ij} is the velocity gradient tensor, S_{ij} and S_{ijkl} are the second- and fourth-order moments of the orientation distribution function, and A, B, C are the material constants specified by the particle aspect ratio. Most constitutive models for dilute and semi-dilute suspensions differ from each other based on how the material coefficients A, B, and C are defined. Recently, the explicit expressions for A, B, and C suggested by different constitutive models have been discussed and briefly reviewed by Lipscomb et al. [14], Altan [27], Tucker [28], and Phan-Thien and Graham [22]. As shown in these studies, the form of the material coefficients simplifies significantly for particles with very small or very large aspect ratios, such as for thin disks and for slender bodies, respectively. For slender bodies, it can be shown that $C \approx B \ll A$; therefore, for dilute suspensions, the viscous stress tensor due to particles, τ_{ij}^{p}, simplifies to

$$\tau_{ij}^{p} = \mu\phi_v A S_{ijkl}u_{kl}, \tag{2}$$

$$A = \frac{a_p^2}{(\ln 2a_p - \frac{3}{2})}, \tag{3}$$

where a_p is the aspect ratio of the fiber. As an alternative, a similar but somewhat less accurate asymptotic value for A can be expressed as [14]

$$A = \frac{a_p^2}{\ln a_p} \tag{4}$$

In semi-dilute suspensions, the average fiber spacing may change between fiber length and diameter, and therefore, a hydrodynamic interaction between the particles exists. For such material systems, an expression similar to Eq. (2) was proposed by Dinh and Armstrong [13] as

$$\tau_{ij}^{p} = \mu \frac{\pi n l^3}{6\ln(2h/d)} S_{ijkl} u_{kl}, \tag{5}$$

where n is the fiber number density, l and d are the length and diameter of the fiber, and h is defined to be the average fiber spacing as

$$h = \begin{cases} (nl)^{-1/2} & \text{for aligned orientations,} \\ (nl^2)^{-1} & \text{for random orientations.} \end{cases} \tag{6}$$

In fact, the average fiber spacing h can be considered to be dependent on the orientation state which changes between the minimum and maximum values corresponding to the randomly oriented and fully aligned fibers, respectively. Recently, Shaqfeh and Fredrickson [29] provided higher order corrections for the coefficient A in both dilute and semi-concentrated suspensions. They also suggested the use of $h = (nl)^{-1/2}$ in Eq. (5) as the first-order approximation regardless of the orientation state. Experimental data towards verification of Eqs. (2) and (5) are rather limited; however, the available experimental studies [14,30,31] suggest that both equations, despite their inherent limitations, are capable of predicting a number of important rheological features observed in both dilute and semi-dilute fiber suspensions. In this paper, following Eqs. (2) and (5), the constitutive equation for suspensions containing slender fibers is taken as

$$\tau_{ij}^{p} = \mu C S_{ijkl} u_{kl} \tag{7}$$

where we choose to define C as a nondimensional suspension parameter which includes the combined effects of volume fraction and fiber aspect ratio. For example, the variation of C as a function of fiber aspect ratio and volume fraction based on dilute suspension models is shown in Fig. 1 (see a similar figure in Ref. [28]). Obviously, the value of C increases considerably for very high aspect ratio fibers even at low volume fractions.

3. Theory and governing equations

3.1. Equations for flow kinematics

The governing momentum equations of a two-dimensional, steady, incompressible flow are expressed in rectangular coordinates as

$$\rho\left(u\frac{\partial u}{\partial x} + v\frac{\partial u}{\partial y}\right) = -\frac{\partial p}{\partial x} + \frac{\partial \tau_{11}}{\partial x} + \frac{\partial \tau_{12}}{\partial y}, \tag{8}$$

$$\rho\left(u\frac{\partial v}{\partial x} + v\frac{\partial v}{\partial y}\right) = -\frac{\partial p}{\partial y} + \frac{\partial \tau_{21}}{\partial x} + \frac{\partial \tau_{22}}{\partial y}, \tag{9}$$

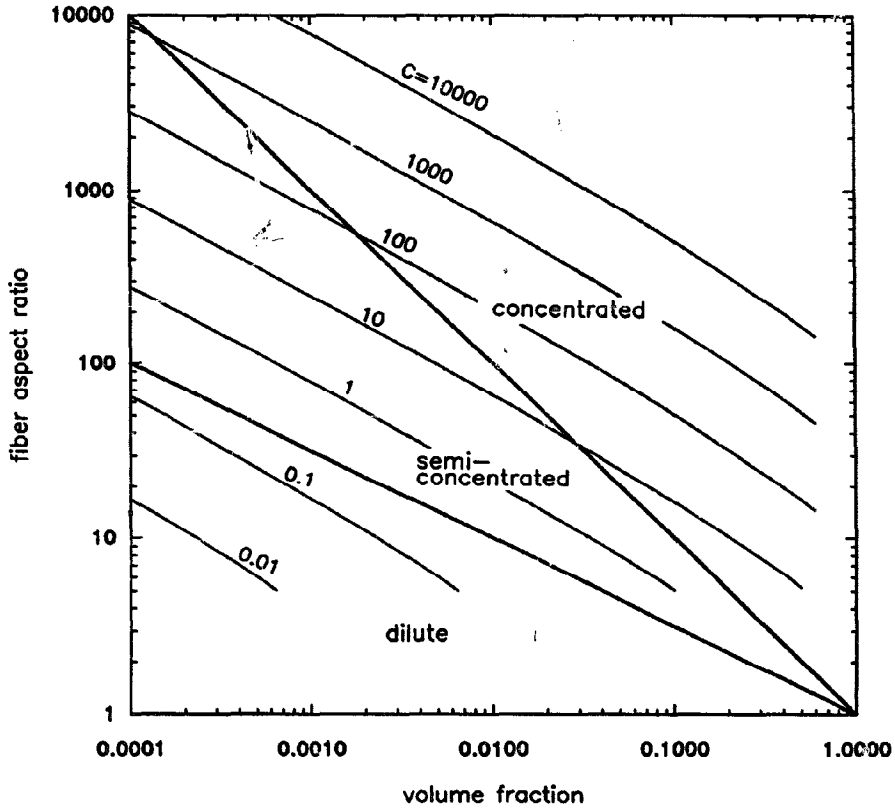

Fig. 1. Variation of nondimensional suspension parameter C in different concentration regions.

where ρ is the density of the fluid, u is the velocity component along the x axis, v is the velocity component along the y axis, p is the hydrostatic pressure, and τ_{ij} are the viscous stress tensor components given in Eq. (1). After introducing Eq. (7) for τ_{ij}^{p} into the Eqs. (8) and (9) and subtracting Eq. (9) from Eq. (8), the governing momentum equation for fiber suspensions can be explicitly written as

$$\rho\left[u\frac{\partial}{\partial x}\left(\frac{\partial u}{\partial y}-\frac{\partial v}{\partial x}\right)+v\frac{\partial}{\partial y}\left(\frac{\partial u}{\partial y}-\frac{\partial v}{\partial x}\right)\right]$$
$$=\mu\left[2\frac{\partial^2}{\partial x\partial y}\left(\frac{\partial u}{\partial x}\right)+\frac{\partial^2}{\partial y^2}\left(\frac{\partial u}{\partial y}+\frac{\partial v}{\partial x}\right)-\frac{\partial^2}{\partial x^2}\left(\frac{\partial u}{\partial y}+\frac{\partial v}{\partial x}\right)-2\frac{\partial^2}{\partial x\partial y}\left(\frac{\partial v}{\partial y}\right)\right]$$
$$+C\left\{\frac{\partial^2}{\partial x\partial y}\left[\frac{\partial u}{\partial x}S_{1111}+\left(\frac{\partial u}{\partial y}+\frac{\partial v}{\partial x}\right)S_{1112}+\frac{\partial v}{\partial y}S_{1122}\right]\right.$$
$$\left.+\frac{\partial^2}{\partial y^2}\left[\frac{\partial u}{\partial x}S_{1112}+\left(\frac{\partial u}{\partial y}+\frac{\partial v}{\partial x}\right)S_{1122}+\frac{\partial v}{\partial y}S_{1222}\right]\right.$$

$$-\frac{\partial^2}{\partial x^2}\left[\frac{\partial u}{\partial x}S_{1112}+\left(\frac{\partial u}{\partial y}+\frac{\partial v}{\partial x}\right)S_{1122}+\frac{\partial v}{\partial y}S_{1222}\right]$$
$$-\frac{\partial^2}{\partial x\partial y}\left[\frac{\partial u}{\partial x}S_{1122}+\left(\frac{\partial u}{\partial y}+\frac{\partial v}{\partial x}\right)S_{1222}+\frac{\partial v}{\partial y}S_{2222}\right]\Bigg\} \tag{10}$$

The geometry and the relevant parameters for the planar channel entry flow are shown in Fig. 2. For such flow problems, it is customary to nondimensionalize the equations by using the half-channel width H as the characteristic length and the uniform inlet velocity U as the characteristic velocity. Hence, the nondimensional parameters are expressed as

$$\bar{x}=\frac{x}{H};\qquad \bar{y}=\frac{y}{H};\qquad \bar{u}=\frac{u}{U};\qquad \bar{v}=\frac{v}{U}. \tag{11}$$

In addition, the stream function Ψ is defined by

$$u=\frac{\partial\Psi}{\partial y};\qquad v=-\frac{\partial\Psi}{\partial x}, \tag{12}$$

and nondimensionalized to be

$$\bar{\Psi}=\frac{\Psi}{HU}. \tag{13}$$

After introducing the nondimensional parameters given in Eqs. (11) and (13), and dropping the bars from nondimensional parameters, Eq. (10) can be written in terms of the stream function as

$$Re\left[\frac{\partial\Psi}{\partial y}\frac{\partial}{\partial x}(P+Q)-\frac{\partial\Psi}{\partial x}\frac{\partial}{\partial y}(P+Q)\right]-\left(\frac{\partial^2 P}{\partial x^2}+\frac{\partial^2 Q}{\partial y^2}+2\frac{\partial^2}{\partial x\partial y}\right)$$
$$=C\left\{\frac{\partial^2}{\partial x\partial y}[(S_{1111}-2S_{1122}+S_{2222})R+(S_{1112}-S_{1222})(Q-P)]\right.$$
$$\left.+\left(\frac{\partial^2}{\partial y^2}-\frac{\partial^2}{\partial x^2}\right)[(S_{1112}-S_{1222})R+S_{1122}(Q-P)]\right\}, \tag{14}$$

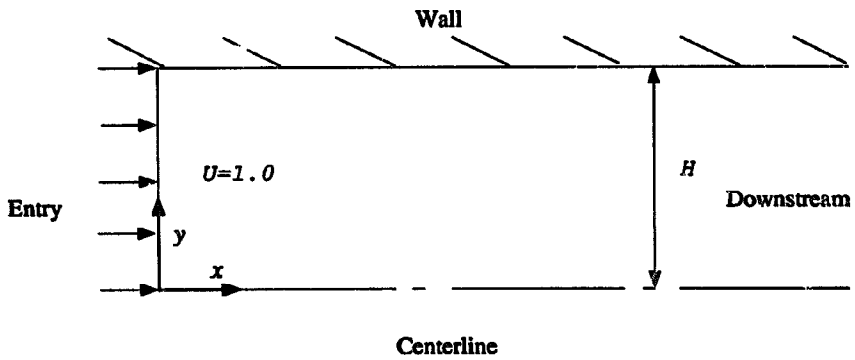

Fig. 2. Planar channel geometry and flow parameters.

where

$$Re = \frac{\rho UH}{\mu}; \qquad P = \frac{\partial^2 \Psi}{\partial x^2}; \qquad Q = \frac{\partial^2 \Psi}{\partial y^2}; \qquad R = \frac{\partial^2 \Psi}{\partial x \partial y}. \tag{15}$$

It should be noted that the Reynolds number, given in Eq. (15), is defined based on the channel length scale and the macroscopic inlet velocity U. In this study, the Reynolds number range is taken to be 0–50 to represent practical processing conditions for fiber suspensions. However, for small particles suspended in the channel, the particle Reynolds number may still be considered as much less than one. Therefore, Stokes flow governs the particle rotation, and consequently, Jeffery's expressions [32] can be utilized to describe the rotation of each particle (a detailed discussion on different scales and Reynolds numbers involved in such multi-scale systems is provided by Batchelor [15]).

Since the channel is symmetric about the centerline, the flow domain is taken to be only half the channel as shown in Fig. 2. Then the boundary condition to the centerline can be expressed as

$$\frac{\partial \Psi}{\partial y} = 0; \qquad \Psi = 0. \tag{16}$$

On the channel wall, a no-slip boundary condition is imposed on the velocity field:

$$\frac{\partial \Psi}{\partial y} = 0; \qquad \Psi = 1. \tag{17}$$

At the inlet, a uniform velocity profile is specified as

$$\Psi = y; \qquad \frac{\partial \Psi}{\partial x} = 0. \tag{18}$$

At the exit, a fully developed velocity profile is expected if the channel is long enough. Hence, the boundary conditions become:

$$\frac{\partial \Psi}{\partial x} = 0; \qquad \frac{\partial^2 \Psi}{\partial x \partial y} = 0. \tag{19}$$

3.2. *Equations for orientation field*

In order to characterize the flow behavior of suspensions, Eq. (14) needs to be solved in conjunction with the equations describing the evolution of orientation structure. Towards this end, the components of the S_{ijkl} tensor need to be determined at each grid point throughout the flow domain. Although a number of different methods exist to evaluate S_{ijkl} components, satisfactory accuracy often requires significant computational effort.

In most of the constitutive models of fiber suspensions, the evolution of orientation field is usually based on the rotation of a single, inertialess ellipsoidal particle

moving affinely with the bulk fluid. The expression for the rotation of such a particle is obtained by Jeffery [32], and can be expressed as

$$\dot{p}_i = (\Omega_{ij} + \lambda D_{ij})p_j - \lambda p_i p_l p_k D_{lk}, \tag{20}$$

$$\Omega_{ij} = \frac{1}{2}\left(\frac{\partial u_i}{\partial x_j} - \frac{\partial u_j}{\partial x_i}\right), \tag{21}$$

$$D_{ij} = \frac{1}{2}\left(\frac{\partial u_i}{\partial x_j} + \frac{\partial u_j}{\partial x_i}\right), \tag{22}$$

where $\dot{p}_i$ is the time rate of change of the unit orientation vector coinciding with the particle's axis of revolution, and Ω_{ij} and D_{ij} represent the vorticity and strain rate tensors, respectively. The parameter λ is a function of particle aspect ratio, a_p, as

$$\lambda = \frac{a_p^2 - 1}{a_p^2 + 1}. \tag{23}$$

However, instead of a single orientation vector, one may choose to utilize an orientation distribution function, $\psi(\vec{p},t)$, to characterize the orientation field. For non-Brownian, rigid fibers, the governing equation for the orientation distribution function is a form of the Fokker–Planck equation and can be written as

$$\frac{\partial \psi(\vec{p},t)}{\partial t} = -\frac{\partial[\dot{p}_i \psi(\vec{p},t)]}{\partial p_i}, \tag{24}$$

where $\dot{p}_i$ is expressed by Eq. (20). Although the definition of the second- and the fourth-order orientation tensors is based on the orientation distribution function as

$$S_{ij} = \langle p_i p_j \rangle = \int p_i p_j \psi(\vec{p})\, \mathrm{d}\vec{p}, \tag{25}$$

$$S_{ijkl} = \langle p_i p_j p_k p_l \rangle = \int p_i p_j p_k p_l \psi(\vec{p})\, \mathrm{d}\vec{p}, \tag{26}$$

the direct use of Eqs. (25) and (26) is not convenient for complex flows due to the difficulties associated with the accurate numerical solution of Eq. (24) throughout the flow domain. Therefore, from Eqs. (25) and (26) alternative orientation evolution equations can be obtained [33–37]. The final expressions are usually in the differential form in which integration over the orientation distribution function is avoided. Using Eqs. (25) and (20), the evolution of the second-order orientation tensor can be expressed as

$$\frac{\mathrm{d}S_{ij}}{\mathrm{d}t} = (\Omega_{im} + \lambda D_{im})S_{mj} + (\Omega_{jm} + \lambda D_{jm})S_{mi} - 2\lambda D_{kl} S_{ijkl}. \tag{27}$$

Similarly, from Eqs. (26) and (20), the expression for the evolution of the fourth-order tensor is obtained as

$$\begin{aligned}\frac{\mathrm{d}S_{ijkl}}{\mathrm{d}t} = {} & (\Omega_{im} + \lambda D_{im})S_{mjkl} + (\Omega_{jm} + \lambda D_{jm})S_{mikl} \\ & + (\Omega_{km} + \lambda D_{km})S_{mijl} + (\Omega_{lm} + \lambda D_{lm})S_{mijk} - 4\lambda D_{rs} S_{ijklrs}.\end{aligned} \tag{28}$$

Eqs. (27 and 28) can be separately used depending on the desired level of orientation description. Eq. (28) is potentially more accurate, and its solution contains the second-order tensor components. However, compared to Eq. (27), solving Eq. (28) would require more computational power. Obviously, both equations contain the unknown higher order orientation tensors which need to be approximated by lower order tensorial components. For homogenous flows where the velocity gradient tensor is spatially uniform, the accuracy and usefulness of various closure approximations have been investigated by many researchers [36–40]. Generally, using such closure approximations can introduce considerable error and, as in the case of linear [33,36] and some hybrid [35,37] closure approximations, may lead to unstable orientation predictions. Similar studies on the accuracy of closure approximations are not available for the complex flows of suspensions, where the encountered problems of numerical stability and convergence [14,20–23,41] may potentially be due to such approximations. Nevertheless, both Eqs. (27) and (28) have been extensively used in complex suspension flows. In particular, quadratic closure approximation has the simplest form and is used most often [20,21,23,41]. For the fourth- and sixth-order orientation tensors, quadratic closure approximations are given as

$$S_{ijkl} = S_{ij}S_{kl}, \tag{29}$$

$$S_{ijklrs} = S_{ijkl}S_{rsmm}. \tag{30}$$

Eqs. (27) and (28), when used with Eqs. (29) and (30), perform reasonably well for the aligned orientation states and predict correct preferred orientation angle values for both finite and infinite aspect ratio fibers [40]. On the other hand, for random or partial particle alignments, the results for individual tensorial components contain significant errors. Such inaccuracies become particularly crucial in the numerical simulation of complex suspension flows where accurate prediction of each S_{ijkl} component is needed regardless of the orientation state and flow kinematics. It should also be emphasized that, the use of Eqs. (29) and (27) together with Eq. (14) to obtain the coupled flow and orientation fields involves using the same closure approximation twice. This approach, although the simplest, does not conserve the required tensorial symmetry for the constitutive models and may lead to inconsistent and erroneous results as shown in Ref. [40]. In a recent article by Szeri and Leal [42], the shortcomings of using closure approximations are also discussed where nonphysical orientation behaviour is observed due to such approximations. Therefore, a more accurate and efficient method to evaluate and describe the orientation state in suspensions needs to be developed. In the next section, we present an alternative technique to describe the orientation field. The technique presented shows that the construction of the orientation distribution function and the subsequent calculation of orientation tensors can be achieved with satisfactory accuracy from the rotational characteristics of relatively few fibers. The technique presented here is very similar to the one proposed by Szeri and Leal [42,43]. In Ref. [42], a theoretical foundation of the so-called double Lagrangian method is developed for two- and three-dimensional orientation fields with Brownian effects.

In a subsequent paper [43], this method was applied to one-dimensional, time dependent pressure driven flow between parallel plates.

3.3. Construction of orientation distribution function

The expression governing the rotation of a single ellipsoidal particle can be used as the basis of constructing the orientation distribution function. An adequate number of orientation angles can be followed in the orientation space, thus forming a Lagrangian approach to orientation evolution. The conformation of these orientation angles can be used to construct the distribution function or its moments with considerable efficiency.

For an arbitrary homogeneous flow, the solution of Eq. (20) with the initial condition for the orientation vector $p_i = p_i^0$ can be shown to be

$$p_i = \frac{E_{ij}p_j^0}{(E_{lm}E_{lj}p_j^0p_m^0)^{1/2}}, \tag{31}$$

where E_{ij} are the components of a particle rotation tensor, defined by

$$\frac{dE_{ij}}{dt} = (\Omega_{ik} + \lambda D_{ik})E_{kj}. \tag{32}$$

Eq. (31) provides the analytical solution of the rotation of the orientation vector, and is valid for both two- and three-dimensional flows and orientation fields. For infinite aspect ratio fibers (i.e., slender fibers) $\lambda = 1$, and Eq. (32) reduces to

$$E_{ij} = \frac{\partial x_i}{\partial x_j^0}, \tag{33}$$

where x_i and x_j^0 are the fluid particle coordinates at times t and t^0 ($t^0 < t$), respectively. Hence, for $\lambda = 1$, E_{ij} is defined as the strain tensor for the undisturbed flow.

In order to determine the particle rotation tensor components in terms of velocity gradients for planar orientations, two sets of differential equations, given by Eq. (32), need to be solved with the initial condition $\boldsymbol{E} = \boldsymbol{I}$ (unit tensor) [44]. Each set contains two coupled ordinary differential equations and can be solved independently. After obtaining analytical solutions of Eq. (32), the orientation vector components can be easily calculated for any initial fiber orientation by using Eq. (31). In order to describe a rheologically meaningful orientation state, the same equations can be used for numerous fictitious fibers with each one starting from a different initial orientation. Then, at any given time, the orientation conformation of these fibers can be utilized to generate the orientation distribution function.

In order to construct the orientation distribution function, one can select non-uniform angular intervals which are based on the angular spacing between two neighboring fibers. The orientation angles of N fibers will specify N different intervals defined within the orientation space. First, consider the orientation angles of N fibers which are given as $\phi_1, \ldots, \phi_{i-1}, \phi_i, \phi_{i+1}, \ldots, \phi_N$, where $0 \le \phi_1 < \cdots < \phi_{i-1} < \phi_i < \phi_{i+1} < \cdots < \phi_N < \pi$. Accordingly, the angular intervals are expressed as

$$\begin{aligned} &\Delta\phi_i = \phi_{i+1} - \phi_i \qquad i = 1 \ldots N-1, \\ &\Delta\phi_i = \pi - \phi_N + \phi_1 \qquad i = N. \end{aligned} \tag{34}$$

Then, the value of the orientation distribution function for the angular interval $\Delta\phi_i$ can be taken to be inversely proportional to that interval as

$$\psi_i \propto \frac{1}{\Delta\phi_i}. \tag{35}$$

Considering that the distribution function for planar orientations satisfies the normalization condition as

$$\int_0^{\pi} \psi(\phi)\, \mathrm{d}\phi = 1, \tag{36}$$

the proper scaling of distribution function values can be performed on Eq. (35),

$$\psi_i = \frac{1}{N\Delta\phi_i}. \tag{37}$$

Obviously, in Eq. (37), each fiber provides a datum point for the construction of the distribution function, and since the data points are mostly at regions with smaller angular intervals (i.e., around the preferred orientation where the curve is steeper), the accurate and efficient construction of the distrubution function is automatically achieved. The efficiency and accuracy of implementing such adaptive methods to evaluate the distrubution function and its moments for non-Brownian suspensions is also emphasized in Ref. [43].

Fig. 3(a) shows the exact and constructed orientation distribution function in simple shear flow for two total shear values (i.e., $\gamma = 2$, and 5). The fiber aspect ratio is taken to be 10 and the exact solution is calculated from [38,44]

$$\psi(\vec{p},t) = \frac{1}{\pi}(\Lambda_{lm}\Lambda_{ij}p_j p_m)^{-1}, \tag{38}$$

where Λ_{ij} is the inverse of the particle rotation tensor E_{ij}. Initially the fibers are taken to be randomly oriented and orientation angles of 45 fibers, which are evaluated from Eqs. (32) and (31), are used to generate the orientation distribution function. Hence, the 45 markers shown in Fig. 3(a) correspond to ψ_i values defined at the midpoint of each angular interval $\Delta\phi_i$. For a total shear of 5, the constructed orientation distribution function is practically indentical with the exact solution except near the peak point. For a total shear of 2, excellent agreement is observed with the exact values throughout the domain. As shown in Fig. 3(a), the markers representing ψ_i are concentrated around the preferred direction which automatically provides an efficient description.

Fig. 3(b) shows the exact and constructed distribution functions for planar elongational flow. Again, the fiber aspect ratio is taken as 10, and starting from random orientation, orientation angles of 45 fibers are used to construct the distribution function. For two different total elongation values (i.e., $\epsilon = 0.5$ and 1.5) shown in Fig. 3(b), excellent agreement is obtained with the exact solution.

It is also found that following fewer fibers does not significantly decrease the accuracy of the constructed orientation distribution function. In fact, only 18 fibers are satisfactorily used to determine both the second- and fourth-order orientation tensor components.

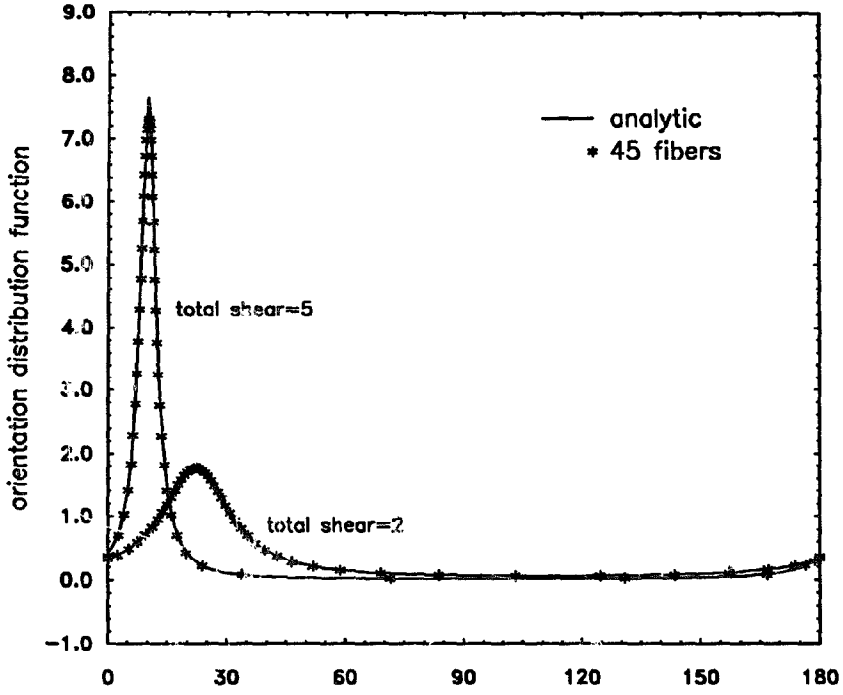

Fig. 3(a).

3.4. Evaluation of orientation tenosrs

After the orientation distribution function is determined, the calculation of orientation tensors can be easily performed from their definitions in Eqs. (25) and (26). Taking ψ as the weighting function, the integration becomes a finite summation that can be calculated numerically. For N fibers, $N+1$ integrals can be evaluated for each one of the S_{ij} components,

$$\begin{aligned} S_{ij} &= \int_0^{\pi} p_i p_j \psi(\phi)\, \mathrm{d}\phi \\ &= \int_0^{\phi_1} p_i p_j \psi(\phi)\, \mathrm{d}\phi + \cdots + \int_{\phi_{m-1}}^{\phi_m} p_i p_j \psi(\phi)\, \mathrm{d}\phi + \cdots + \int_{\phi_N}^{\pi} p_i p_j \psi(\phi)\, \mathrm{d}\phi. \end{aligned} \tag{39}$$

Similarly, for the S_{ijkl} components, the integrals become

$$\begin{aligned} S_{ijkl} &= \int_0^{\pi} p_i p_j p_k p_l \psi(\phi)\, \mathrm{d}\phi = \int_0^{\phi_1} p_i p_j p_k p_l \psi(\phi)\, \mathrm{d}\phi + \cdots \\ &\quad + \int_{\phi_{m-1}}^{\phi_m} p_i p_j p_k p_l \psi(\phi)\, \mathrm{d}\phi + \cdots + \int_{\phi_N}^{\pi} p_i p_j p_k p_l \psi(\phi)\, \mathrm{d}\phi. \end{aligned} \tag{40}$$

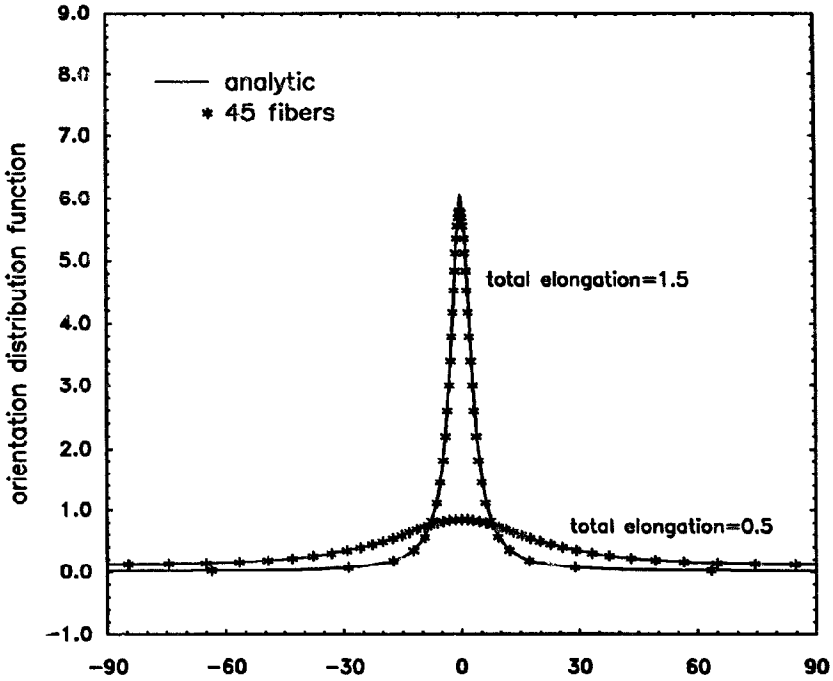

Fig. 3(b).

Fig. 3(a). Orientation distribution function for simple shear flow constructed from the orientation angles of 45 fibers: $a_p = 10$; total shear, 2,5. (b) Oreintation distribution function for planar elongational flow constructed from the orientation angles of 45 fibers: $a_p = 10$; total elongation, 0.5,1.5.

Among several techniques, the individual integrals are efficiently calculated by the trapezoid rule. Higher order numerical integration schemes can also be implemented; however, increased computational time and limited improvement in the accuracy do not warrant their use in this context.

$$\int_{\phi_{m-1}}^{\phi_m} p_i p_j \psi(\phi)\, \mathrm{d}\phi = \tfrac{1}{2}\{[p_i p_j \psi(\phi)]_m + [p_i p_j \psi(\phi)]_{m-1}\}(\phi_m - \phi_{m-1}), \tag{41}$$

$$\int_{\phi_{m-1}}^{\phi_m} p_i p_j p_k p_l \psi(\phi)\, \mathrm{d}\phi = \tfrac{1}{2}\{[p_i p_j p_k p_l \psi(\phi)]_m + [p_i p_j p_k p_l \psi(\phi)]_{m-1}\}(\phi_m - \phi_{m-1}). \tag{42}$$

It should be noted that to evaluate Eqs. (39) and (40), the distribution function value at $\phi = 0$ needs to be known. This can be obtained by considering the distribution function values of two points, ψ_1 and ψ_N, and utilizing a linear fit that would yield $\psi(0)$.

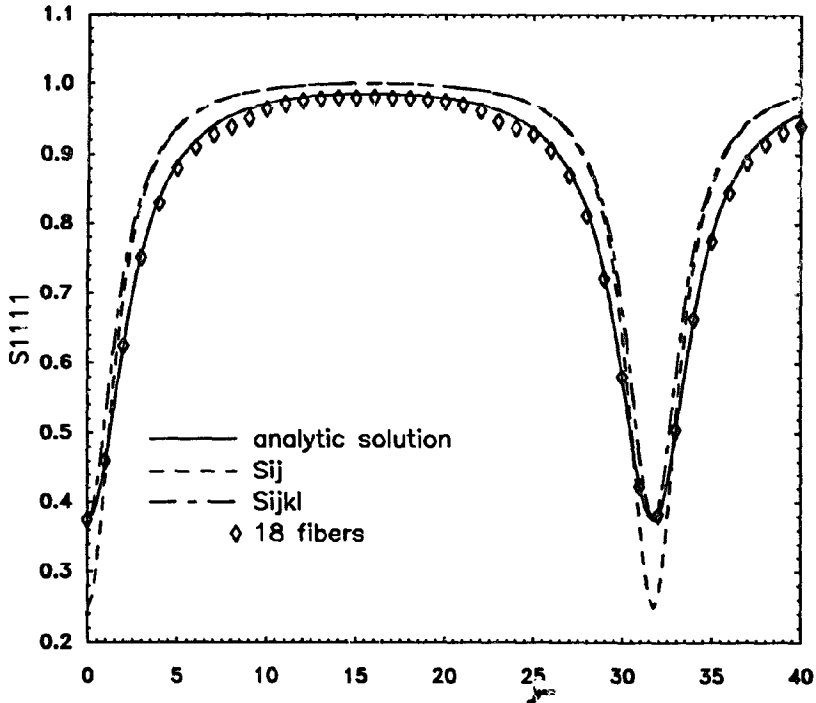

Fig. 4(a).

Before implementing this method in complex flows, a comparative study is performed for simple shear and planar elongational flows to investigate the accuracy and the efficiency of this method. Comparisons are performed with the exact solutions[1] and with the results obtained from both orientation evolution equations expressed by Eqs. (27) and (29) (i.e., denoted by S_{ij}), and by Eqs. (28) and (30) (i.e., denoted by S_{ijkl}).

Simple shear flow

It is well known that the rotation of finite aspect ratio fibers in simple shear flow is periodic. As a corollary to this, the orientation structure, described by S_{ijkl} components, is also periodic. This is observed in Figs. 4(a) and 4(b) that show the predictions for S_{1111} and S_{1122} for a fiber aspect ratio of 10. The orientation angles of 18 fibers are used to determine the tensor components a process which is

[1] Exact solutions for the planar orientation tensors in arbitary homogeneous flows are given in Ref. [40]. Simplified expressions used in this paper for simple shear and planar elongational flows are given in the Appendix.

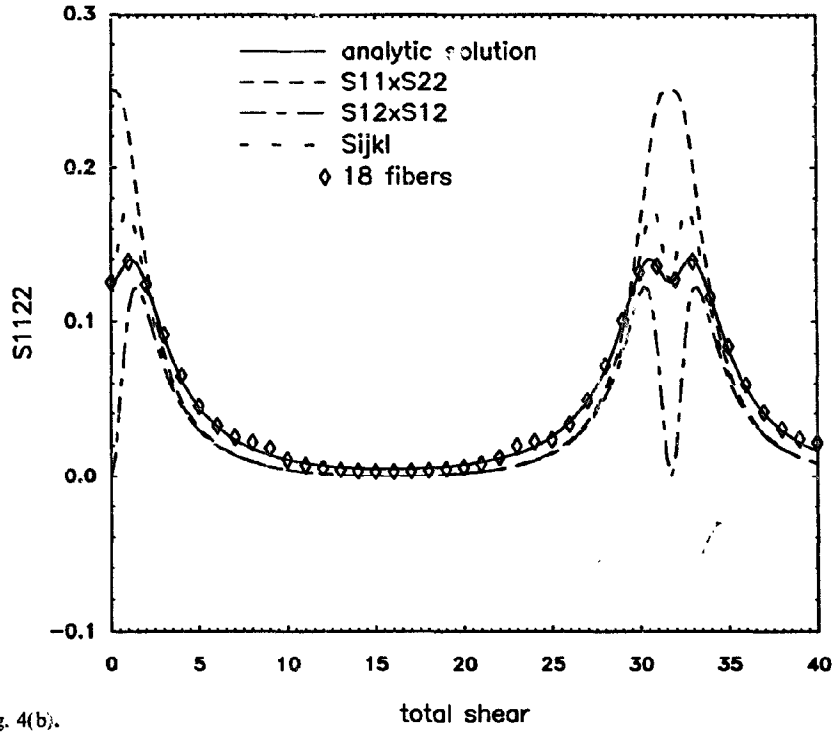

Fig. 4(b).

Fig. 4(a). Fourth-order tensor components S_{1111} as a function of total shear: $a_p = 10$. (b) Fourth-order tensor component S_{1122} as a function of total shear: $a_p = 10$.

computationally much faster than solving evolution equations. The results obtained by following only 18 angles are in excellent agreement with the exact solutions. It is observed that all the details and the periodicity of the orientation structure are captured with this method. Since the results are extremely close to the exact values, markers are used in Figs. 4(a) and 4(b) for clarity. However, the results from both evolution equations contain significant inaccuracies. It should be noted that the implementation of the fourth-order quadratic closure approximation cannot be uniquely defined in Fig. 4(b). Specifically, since $S_{1122} = S_{1212}$, two different quadratic approximations can be written as

$$S_{1122} = S_{11}S_{22}, \qquad S_{1122} = S_{12}S_{12}. \tag{43}$$

Therefore, the results obtained from both of these approximations are presented for S_{1122}.

A similar level of accuracy is obtained for infinite aspect ratio fibers. For this case, the orientation structure is not periodic and fibers attain a steady perfect

alignment along the flow direction. The steady orientation state is correctly predicted by both evolution equations; however, at low total shear values, where the fibers are moderately aligned, significant discrepancies with the exact solutions are observed.

Such comparisons are also performed for the other nonzero components of the fourth-order tensor (i.e., S_{1112}, S_{1222}, and S_{2222}) where following 18 orientation angles yields much better results compared to evolution equations. The stability of predictions is also tested at high deformations for both finite and infinite aspect ratio fibers. For all the values of total shear, the errors generated by following 18 or more fibers are found to be less than 1%, whereas the errors from evolution equations are observed to be as much as 300%.

Planar elongation flow

Similar to shear flow predictions, the orientation angles of 18 fibers are used to determine all nonzero S_{ijkl} components (i.e., S_{1111}, S_{1122}, and S_{2222}). In planar elongational flow, the orientation structure is not periodic, and the fibers align quickly in the flow direction regardless of the aspect ratio. Fig. 5 shows the

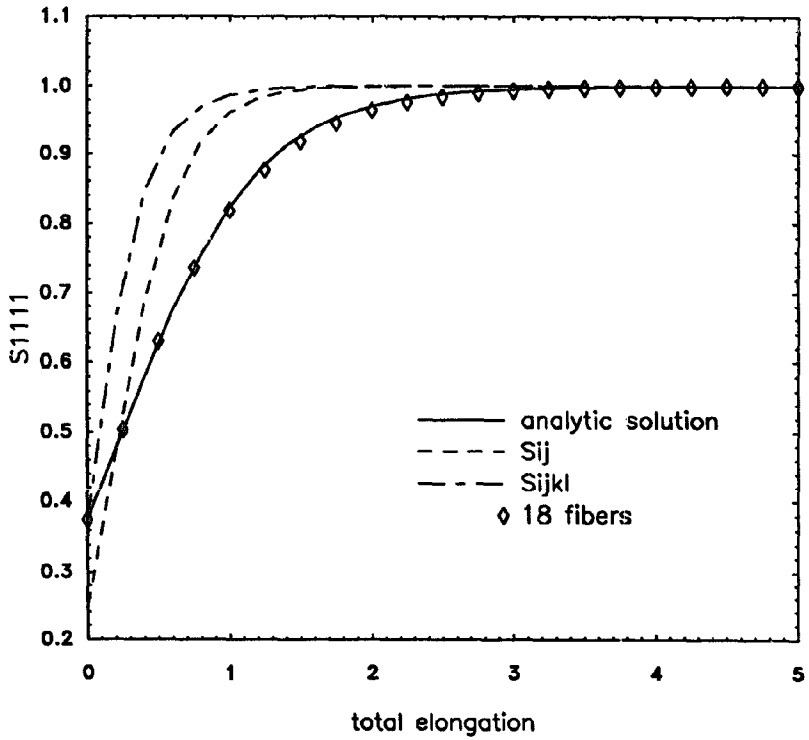

Fig. 5. Fourth-order tensor component S_{1111} as a function of total elongation: $a_p = 10$.

predictions of S_{1111} for a fiber aspect ratio of 10. As exemplified by Fig. 5, the proposed method depicts excellent agreement with the exact results for all S_{ijkl} components. On the other hand, for all three nonzero S_{ijkl} components, both evolution equations yield inaccurate results for moderately aligned fibers. Furthermore, S_{1122} is erroneously predicted to be zero when the quadratic closure approximation is used as $S_{1122} = S_{12}S_{12}$.

Stability of predictions is also tested at high deformations for both finite and infinite aspect ratio fibers. At high total elongations, accurate and stable results are obtained from both evolution equations and from the new technique using discrete fibers. If orientation angles of 18 or more fibers are used, the error is always less than 1%. However, at low elongation values, the evolution equations are in error by as much as 30%.

The method described in this section can be easily utilized in the numerical simulation of complex suspension flows, and as demonstrated in Figs. 3–5, performs much better than differential evolution equations in predicting S_{ijkl} components. As opposed to closure approximations, there is no inherent approximation involved in its development, and its numerical implementation is rather straightforward. In addition, inaccuracies involved are numerical in nature and may become significant only when an inadequate number of data points is selected (i.e., fibers followed in the orientation space) to form an orientation structure. We believe that this method can also be applied to recirculating flows. The complex orientation patterns of rigid particles in two- and three-dimensional recirculating flows was analyzed in detail by Szeri [45]. In accordance with the available theory, the orientation structure can be determined throughout the circulation regions and later utilized in the numerical solution of complex suspension flows in an Eulerian reference frame.

4. Steady velocity profile in a channel

Before attempting to solve the governing flow and orientation numerically, it is of importance to investigate the steady velocity profile. The enhancement of the shear viscosity due to the presence and the tumbling of the fibers needs to be throughly understood. It is well known that fibers with infinite aspect ratio reach a perfect alignment with the flow in the channel downstream. At this infinite-aspect-ratio limit, the fiber tumbling ceases and a stable parabolic profile develops provided that the fibers are uniformly dispersed. However, at higher fiber concentrations, particle diffusion across the streamlines exists which leads to a nonuniform particle concentration across the channel. Such concentration variations, naturally generate a nonparabolic profile which is often observed to be similar to a plug flow.

The steady flow behavior of finite-aspect-ratio fibers can be analyzed by simplifying the governing momentum equation as

$$\frac{dp}{dx} = \mu \frac{d}{dy}\left[(1 + CS_{1122})\frac{du}{dy}\right]. \tag{44}$$

Eq. (44) cannot be readily solved without analyzing the behavior of S_{1122}. The value of S_{1122} is periodic and can be determined as a function of the aspect ratio and the total shear γ a particle has experienced. Consequently, the variation of S_{1122} with respect to the y coordinate is dictated by the variation of total shear across the channel width. One can show that as x goes to infinity, the difference in total shear experienced by two neighboring points on the y axis also goes to infinity. Therefore, in the downstream channel, the average value of S_{1122} can be used across the channel. For planar orientation, the average value of S_{1122} can be calculated as

$$\bar{S}_{1122} = \frac{1}{\gamma_T} \int_0^{\gamma_T} S_{1122}(\gamma)\, d\gamma = \frac{a_p}{2(1+a_p)^2}, \tag{45}$$

where γ_T is the period of S_{1122} and is given as

$$\gamma_T = \frac{a_p^2 + 1}{a_p}\pi. \tag{46}$$

After using Eq. (45) in Eq. (44), the fully developed profile can be expressed as

$$u(y) = \frac{1}{\mu\{1 + C[a_p/2(1+a_p)^2]\}} \frac{1}{2}\frac{dp}{dx}(y^2 - 1). \tag{47}$$

Hence, Eq. (47) represents a parabolic fully developed profile with an effective viscosity μ^* dependent on the aspect ratio and C values as

$$\mu^* = \mu(1 + C\bar{S}_{1122}) = \mu\left[1 + C\frac{a_p}{2(1+a_p)^2}\right]. \tag{48}$$

As shown in Eq. (48), the enhancement of the shear viscosity due to the tumbling of the fibers is accounted for by the term $a_p/2(1+a_p)^2$, and if C is kept constant, the increase in aspect ratio would lower the effective viscosity due to less frequent tumbling. However, as Eqs. (2)–(6) illustrate, C is a nondimensional parameter that depends on the fiber volume fraction and the aspect ratio, and if the fiber aspect ratio is increased, one needs to decrease the volume fraction to keep C constant. In the dilute concentration regime, if Eqs. (2) and (4) are used slender fibers, the effective viscosity μ^* can be expressed as

$$\mu^* = \mu\left[1 + \phi_v \frac{a_p^3}{2(1+a_p)^2 \ln a_p}\right]. \tag{49}$$

Hence, if the fiber volume fraction is kept constant in dilute suspensions (i.e., $\phi_v < 1/a_p^2$), effective viscosity is increased by increasing the fiber aspect ratio.

5. Numerical technique

5.1. Stream function

The governing momentum equation (14) is discretized by a standard second-order accurate, conservative finite difference formulation. The grid generated

throughout the channel is concentrated toward the channel entry by using an exponential coordinate transformation along x given as $x^* = x^r$. After trying $r = 1-1.6$, efficient and accurate solutions are obtained using $r = 1.5$ for all the numerical results presented in this study. The Gauss–Seidel explicit iteration technique with a relative convergence criterion, $c_1 = 1 \times 10^{-6}$ is utilized to determine the stream function values at the interior nodal points. The imaginary nodal points outside the flow domain are updated using the solution dependent boundary conditions after completing each iteration throughout the inner nodes. A number of different meshes with 21×11, 31×16, 41×21, 51×31, and 61×31 grid points are utilized, and the mesh with 41×21 grid points is found to yield accurate results with reasonable computational effort. In addition, since the entry length depends on the suspension parameter C, and the Reynolds number Re, at least three runs with different channel lengths are performed to ensure a fully developed condition is achieved before imposing such conditions downstream. Hence, the channel aspect ratio used in the numerical solution is increased from 8 to 240 as the C and Re values are increased.

5.2. Orientation field

In order to solve Eq. (14), five components of the S_{ijkl} tensor need to be known. Since the trace of the second-order tensor S_{ij} is unity, only four of the S_{ijkl} components are independent. As discussed earlier, using a number of orientation angles to construct S_{ijkl} values yields much superior results compared to using second- or fourth-order evolution equations. The behaviour of these three methods is also studied in the channel entry flow in addition to comparisons for simple shear and planar elongational flows provided before.

In all these different solution methods for the orientation field, the S_{ijkl} values at each grid point are determined by a Lagrangian approach in the flow domain. In other words, the orientation equations are solved along particle pathline. In order to improve accuracy, the pathlines terminating at each grid point are constructed. Then, starting from the inlet, the orientation evolution along that particular pathline is determined by using local velocity gradients. This tracing method is particularly suitable for deformation dependent constitutive models and is implemented for all three solution methods for the orientation field. The tracing method is also employed for the centerline (i.e., symmetry axis) as described above. The acceleration of the fluid on the centerline leads to a preferred orientation along the flow direction with a high degree of alignment. Although the specification of orientation field on the channel wall is not needed to determine the orientation evolution throughout the channel, the numerical solution of stream function requires some orientation information on the wall. To alleviate this problem, a perfect alignment given as

$$S_{1111} = 1; \qquad S_{1112} = S_{1122} = S_{1222} = S_{2222} = 0, \tag{50}$$

is specified at the grid points on the channel wall. At the channel entry, together with the uniform velocity profile, fibers are specified to be randomly oriented. Using S_{ij} components, the random inlet condition can be written as

$$S_{11} = 0.5; \qquad S_{22} = 0.5; \qquad S_{12} = 0. \tag{51}$$

Similarly, for S_{ijkl},

$$S_{1111} = S_{2222} = \tfrac{3}{8},$$
$$S_{1122} = \tfrac{1}{8}, \tag{52}$$
$$S_{1112} = S_{1222} = 0.$$

Random orientation is also represented by using uniform angular intervals for fictitious fibers. For example, at the channel inlet, the angular interval between 45 randomly oriented fictitious fibers is specified to be 180°/45.

5.3. Solution algorithm

The coupled solution of the velocity and orientation fields is achieved by an iteration scheme between the stream function and the orientation structure. Based on the change in stream function values after each iteration, the solution algorithm adopts a second relative convergence criterion, c_2. The numerical algorithm can be briefly summarized as follows.

(1) Initially, the stream function is solved from Eq. (14) for the zero-volume-fraction limit to start the iterations. The velocity field is that of a Newtonian fluid.

(2) The orientation structure, specified by S_{ijkl} components, is evaluated at each grid point by tracing the particles along their pathlines.

(3) Utilizing the required suspension parameter C, the stream function is solved with the orientation structure determined in step 2.

(4) The stream function values obtained in step 3 are compared with the values obtained before. If the convergence criterion c_2 is satisfied, then the final stream function and the orientation structure are obtained. Otherwise, step 2 is repeated and a new orientation structure is calculated, thus continuing the literation.

Compared to criterion c_1 used in the Gauss–Seidel iterations, a higher value for c_2 needs to be used. Therefore, the value of c_2 is selected to be 1×10^{-4}. The number of iterations necessary between the flow and the orientation field increased steadily as the C value is increased, and for most cases, the final converged solution is obtained after 5–45 iterations.

6. Results

6.1. Comparisons of orientation solution techniques

The planar channel entry flow of slender, rigid, and neutrally buoyant fibers suspended in a Newtonian fluid is studied by using three different techniques to solve the orientation field. The main emphasis in this section is to determine the accuracy and the stability of these methods in a complex suspension flow where the presence of particles significantly affects the flow kinematics. In order to compare the three different solution methods, the results are presented for $C = 30$ and $Re = 50$ among a number of computer runs performed for various C and Re values.

Fig. 6(a) shows the velocity profile at half-channel-width downstream (i.e., $x = 1$). The solid line represents the profile obtained by following 90 orientation angles (i.e., denoted by 90 fibers), whereas the dashed lines show the results obtained

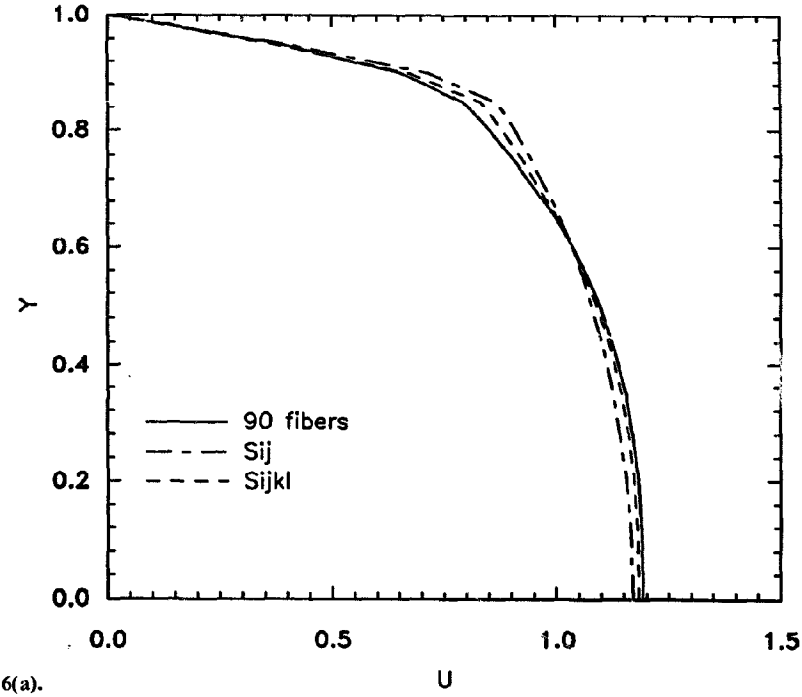

Fig. 6(a).

from the differential evolution equations for the second- and the fourth-order orientation tensors with quadratic closure approximations (i.e., denoted by S_{ij} and S_{ijkl}, respectively). As Fig. 6(a) indicates, all the three methods predict qualitatively similar profiles across the channel at $x = 1$. However, some discrepancies are observed in Fig. 6(a); in particular, starting from the centerline, 5–15% variations in the velocity profiles exist across the channel width. Although these variations seem to be minimal in the velocity profile, S_{11} predictions (i.e., in a sense, the degree of alignment in the flow direction) differ 20–35% along the channel length as shown in Fig. 6(b). Fig. 6(b) depcits S_{11} values only up to $x = 40$ since most of the orientation transients take place near the entry. After $x = 40$, a high degree of alignment in the flow direction is achieved, and the difference between S_{11} predictions is reduced to less than 5%. Overall, both evolution equations are observed to overpredict the degree of alignment. As a result, the evolution equations for the second- and the fourth-order tensors inaccurately predict a much faster development of the flow and the orientation fields.

Fig. 6(c) depicts the S_{11} values obtained from three different mesh sizes. It is clearly observed that the S_{11} results are not mesh dependent and that, as stated in Section 5.1, a mesh with 41 × 21 grid points provides adequate accuracy. Mesh dependence of the other components of the orientation tensors and the velocity field throughout the flow domain is also found to be similar to that of S_{11}.

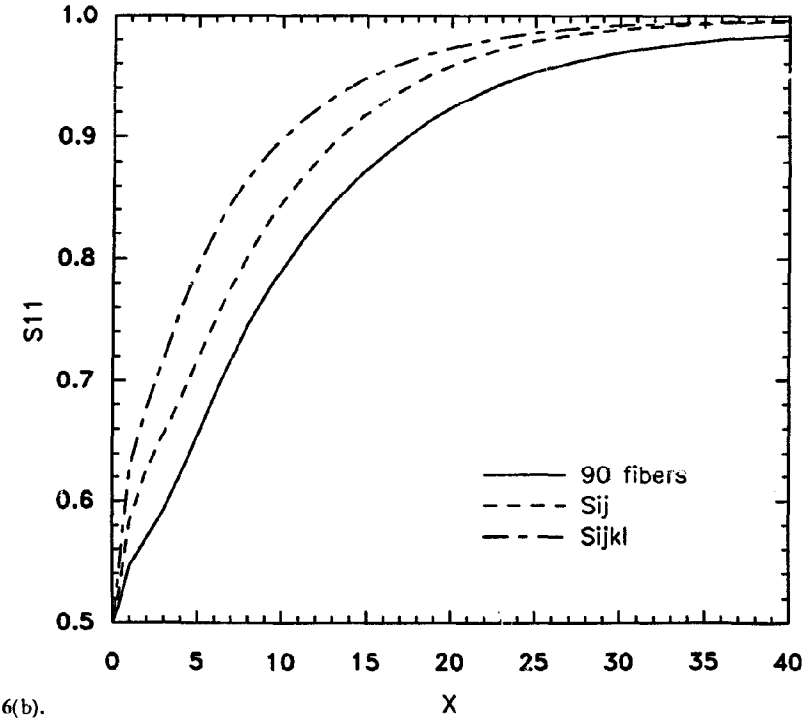

Fig. 6(b).

It should be noted that for C values higher than 30, converged solutions are not obtained from both evolution equations for the second- and the fourth-order tensors. The iterations between the stream function and the orientation field do not satisfy the relative convergence criterion c_2, and the maximum error does not asymptotically approach a minimum value. Such numerical stability problems for higher C values are also encountered by a number of previous studies which (a) utilized the evolution equations for the second- and the fourth-order tensors [21–23,41], or (b) used a more simplistic approach by assuming fibers are perfectly aligned along the streamlines [14,20]. However, following the conformation of the orientation structure through discrete orientation angles does not lead to any stability or convergence problems, even at much higher C values. Therefore, one may conclude that the approximations involved in the calculation of the orientation structure may be one of the reasons for the stability problems encountered in anisotropic suspension flows.

In order to determine the number of fibers that need to be traced, a number of computer runs are performed by following 18, 36, 45, and 90 fibers, and the accuracy obtained from 45 fibers is found to be adequate for all the cases. The improvement in accuracy by using 90 fibers is less than 0.5% in most cases which does not justify the increased computational effort. Consequently, in all the other

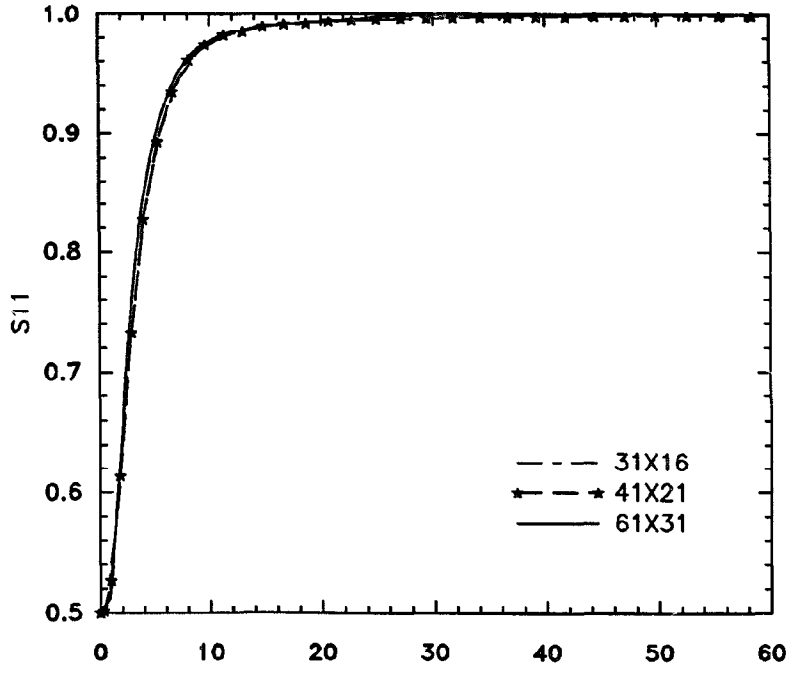

Fig. 6(c)

Fig. 6(a). Comparison of velocity profiles obtained from different solution techniques: $x = 1$; $Re = 50$; $C = 30$. (b) Comparison of S_{11} obtained from different solution techniques: $y = 0.3$; $Re = 50$; $C = 30$. (c) Comparison of S_{11} obtained from different meshes: $y = 0.6$; $Re = 50$; $C = 30$.

results provided in this section, 45 orientation angles are utilized to characterize the orientation evolution.

6.2. *Velocity and orientation profiles*

The velocity profiles at one channel-width downstream (i.e., $x = 2$) are shown in Figs. 7(a) and 7(b) for $C = 0$ and 15, respectively. Fig. 7(a) illustrates the well-known behavior of a Newtonian fluid at $C = 0$. For $Re = 0$, the flow is almost fully developed with a parabolic profile at $x = 2$; whereas for $Re = 50$, the flow is not yet developed, and the concavity of the velocity profile near the midsection of the channel is observed. As the C value is increased to 15, the effect of the Reynolds number on the flow kinematics diminishes as shown in Fig. 7(b). Hence for higher particle concentrations, the development of the velocity profile is retarded, the concavity in the profile is lost, and the suspension behaves similarly to a plug flow. For $C = 30$ and 60, these effects are even more pronounced, and the effect of the Reynolds number on the velocity profile becomes negligible compared to that of C.

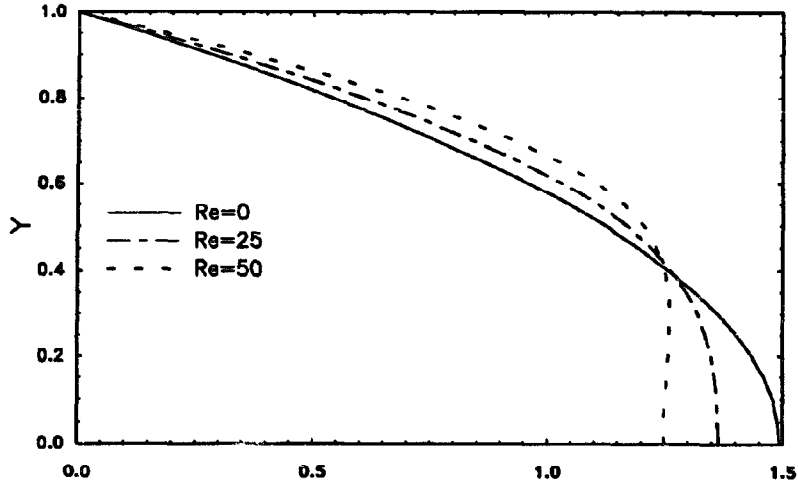

(a)

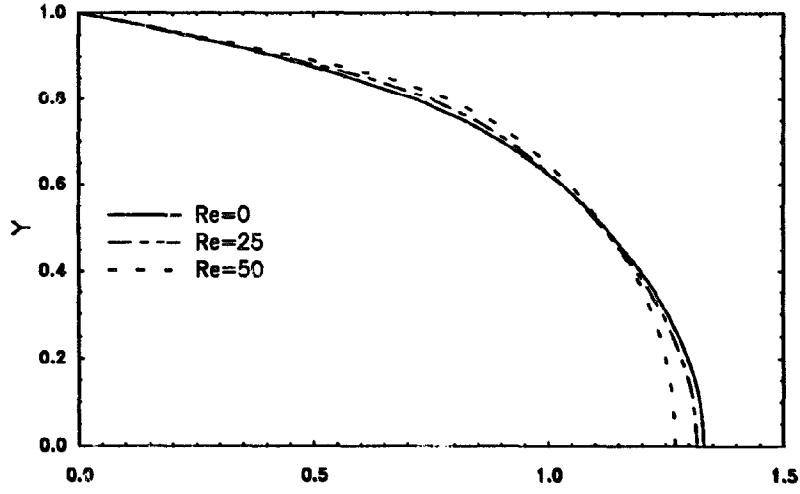

(b)

Fig. 7(a). Velocity profiles across the channel at $x = 2$ for $C = 0$. (b) Velocity profiles across the channel at $x = 2$ for $C = 15$.

The effect of the fibers on the flow kinematics at $x = 2$ can be clearly observed in Figs. 8(a) and 8(b) for $Re = 0$ and 25, respectively. In particular, the C value is found to affect the development of the flow significantly for $Re = 0$ compared to $Re = 25$. For higher C values (i.e., $C = 90$), Re does not affect the flow and both figures yield nearly the same profile.

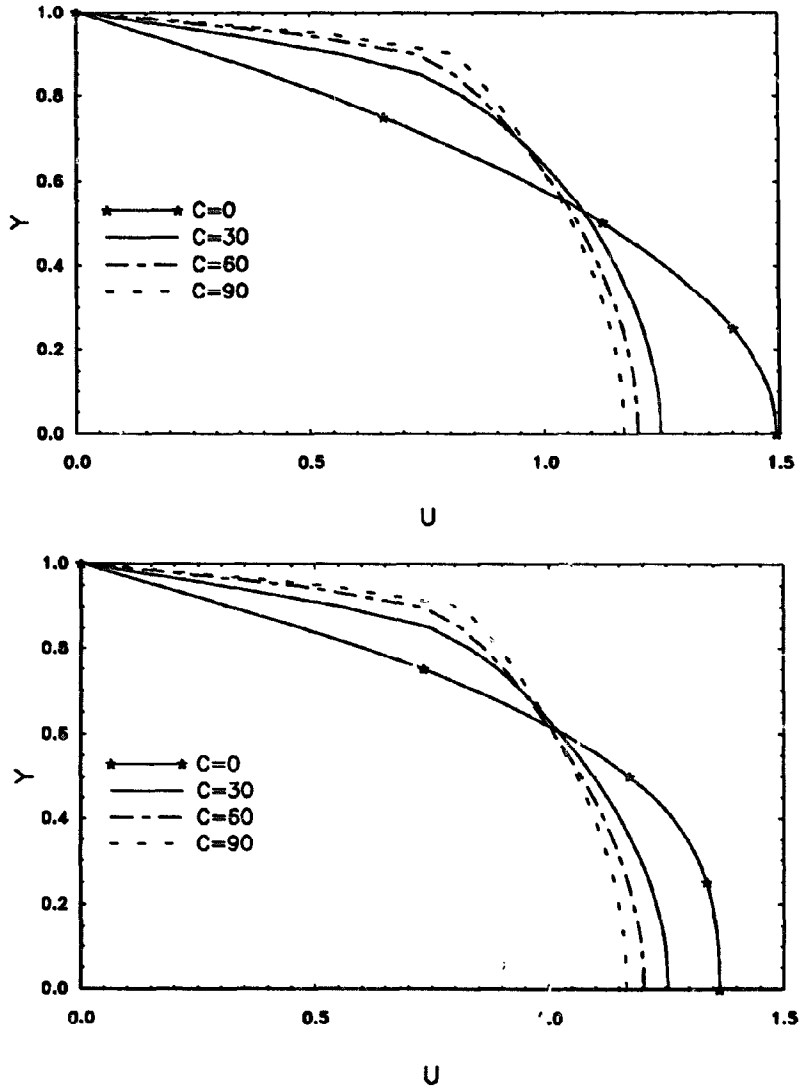

Fig. 8(a). Velocity profiles across the channel at $x = 2$ for $Re = 0$. (b)Velocity profiles across the channel at $x = 2$ for $Re = 25$.

Fig. 9(a) and 9(b) show the S_{11} values along the channel length for different C and Re values. As in the case of velocity profiles, the Reynolds number affects the orientation profile significantly at $C = 0$. S_{11} increases steadily and approaches 1 along the channel length. An increase in C or Re retards the orientation development; however, for higher C values, the effect of the Reynolds number on the

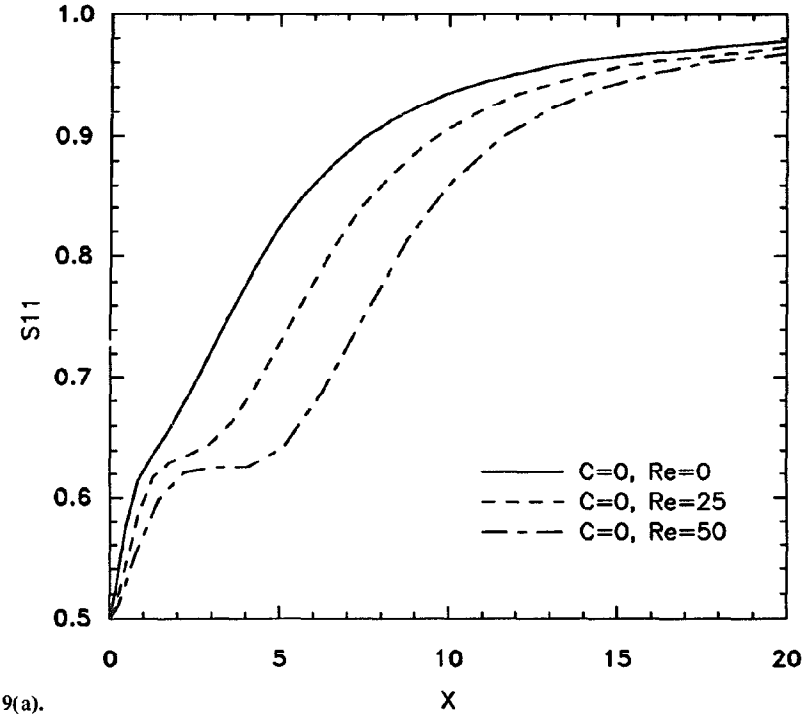

Fig. 9(a).

orientation profile is decreased. Further downstream (i.e., $x > 20$), the flow and the orientation fields approach to a fully developed profile. The rate of the flow and orientation development is mainly dependent on the value of C and can be very slow for high C values. Eventually, the flow attains a parabolic profile in the case of uniformly dispersed slender fiber suspensions. At the same time, the rotational speed of the fibers gradually decreases after a few channel-widths downstream where almost perfect alignment with the flow is obtained.

6.3. Fully developed length

From the numerical solution of suspension flows in a planar channel, it is of interest to investigate the length scale at which the flow becomes fully developed. The location at which 95% of the fully developed centerline velocity is obtained is shown in Fig. 10(a) as a function of C for $Re = 0$, 25, and 50. In Fig. 10(a), the entry length is shown to be almost linearly proportional to the C values for $C \gtrsim 10$. For $C < 4$, the entry length is strongly dependent on the Reynolds number, whereas for $C > 4$, the entry length is mainly dependent on C. For example, for $C = 30$ and $Re = 25$, the 95% fully developed length is increased by 75% by boudling the C, whereas doubling Re only increases the entry length by 6%. Similar observations

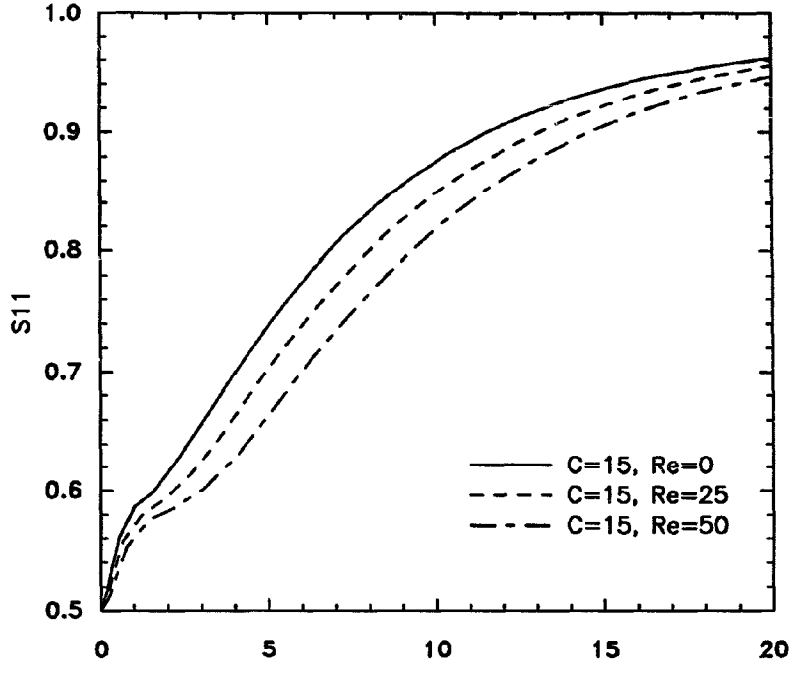

Fig. 9(b).

Fig. 9(a). S_{11} profiles along the channel at $y = 0.3$ for $C = 0$. (b) S_{11} profiles along the channel at $y = 0.3$ for $C = 15$.

can be made based on locations of the 98% fully developed centerline velocity. However, the difference between the 95% and 98% fully developed lengths is quite significant, and in many cases, more than 100%. For instance, the 95% fully developed entry length is 52–58 half-channel widths downstream for $C = 60$ and $0 \leq Re \leq 50$; however the 98% fully developed profiles are reached only after 118–124 half-channel widths downstream for the same C and Re values. This slow flow development is basically due to the decrease in the rotation rate of the fibers. As the alignment of the fibers is increased along the flow, the rotation rate is reduced and the maximum orientation angle asymptotically approaches 0°. In this study, in order to obtain the locations of the 98% fully developed centerline velocity accurately, the channel aspect ratio is selected to be high enough to achieve a profile more than 99% fully developed. For $C = 90$, a channel aspect ratio equal to or more than 240 is found to be adequate.

If the second- and the fourth-order orientation evolution equations are used to calculate S_{ijkl} compenents, the predictions of entry lengths change as shown in Fig. 10(b). Since both differential evolution equations with the quadratic closure approximation lead to faster fiber alignment along the flow, the predicted entry

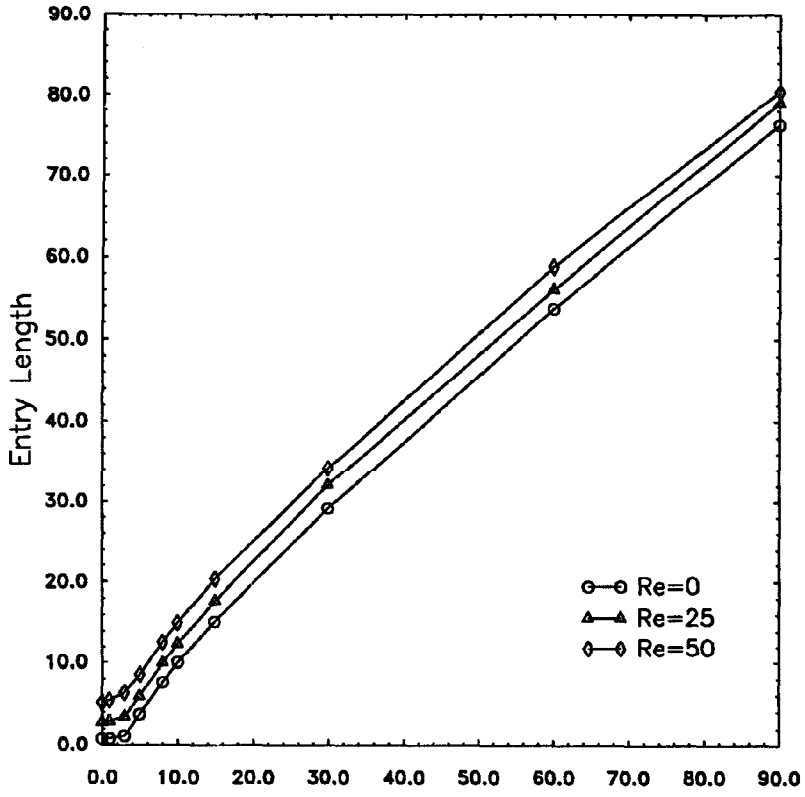

Fig. 10(a).

lengths are substantially shorter than the actual numbers. The 95% and 98% fully developed lengths are underpredicted by the evolution equations by 30–60% for $Re = 0$. Similar behaviors are also observed for $Re = 25$ and 50. It should be noted that, in Fig. 10(b), C is taken only up to 30 since, as explained before, converged solutions are not obtained from evolution equations for higher C values.

6.4. Pressure drop

The pressure gradients throughout the channel can be calculated from the converged stream function values by using

$$\frac{\partial P}{\partial x} = \left(\frac{\partial \tau_{11}}{\partial x} + \frac{\partial \tau_{12}}{\partial y}\right) - Re\left(u\frac{\partial u}{\partial x} + v\frac{\partial u}{\partial y}\right), \tag{53}$$

$$\frac{\partial P}{\partial y} = \left(\frac{\partial \tau_{21}}{\partial x} + \frac{\partial \tau_{22}}{\partial y}\right) - Re\left(u\frac{\partial v}{\partial x} + v\frac{\partial v}{\partial y}\right), \tag{54}$$

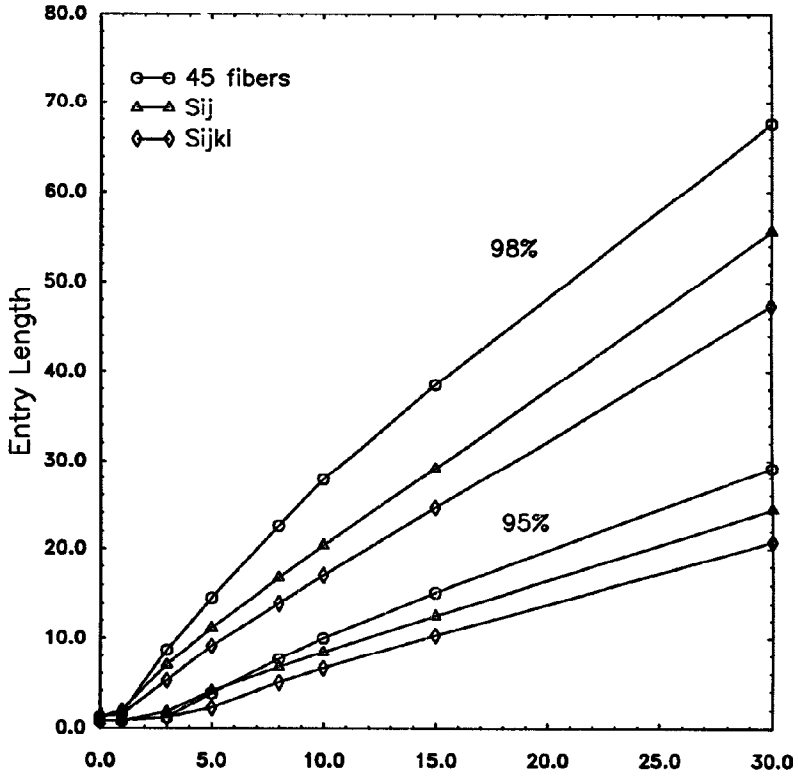

Fig. 10(b).

Fig. 10(a). Entry length for the 95% fully developed centerline velocity. (b) Comparison of the entry lengths obtained from different methods for $Re = 0$.

where the nondimensional pressure, P, is defined as

$$P = \frac{Hp}{U\mu}. \tag{55}$$

For a dilute suspension of slender fibers, where $\phi_v \ll 1$ and $a_p \gg 1$, the asymptotic values of downstream pressure gradients can be written as $dP/dx = -3$ and $dP/dy = 0$.

In Fig. 11, the pressure drop on the centerline (i.e., $dP/dx|_{y=0}$) along the channel length is shown for $Re = 0$. As Fig. 11 indicates, for $Re = 0$ and $C = 0$, the pressure drop approaches its steady value much faster compared to $C = 30$ and 60. In addition, for high C values, pressure drop is considerably increased throughout the channel. In particular, near the channel inlet, the pressure drop is increased between

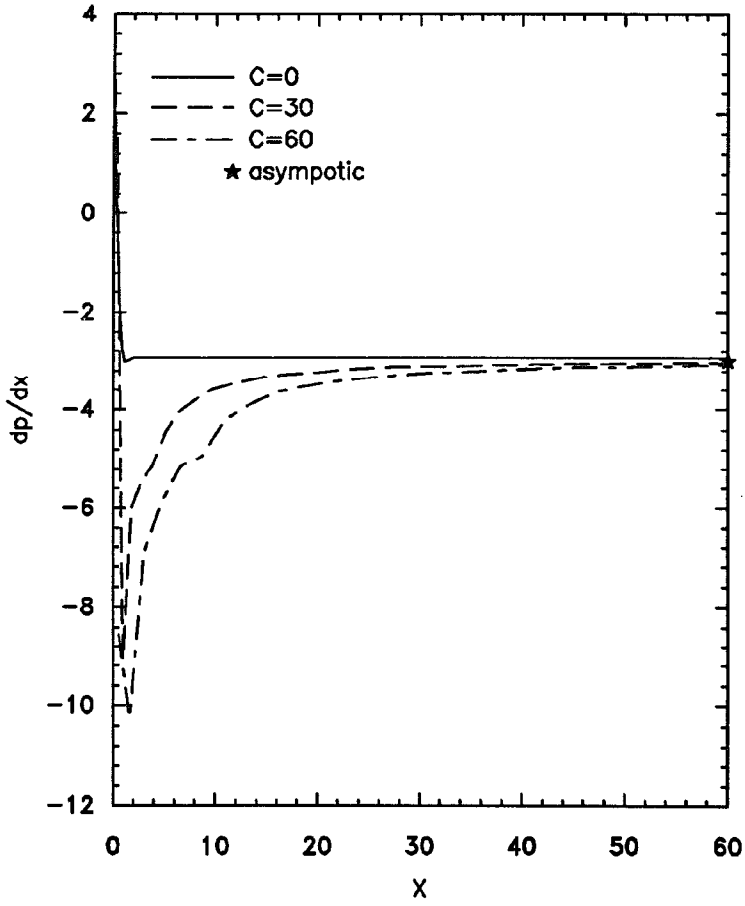

Fig. 11. Variation of the pressure gradient, $\partial P/\partial x$, along the channel at $y = 0.0$ for $Re = 0$.

50 and 300% depending on C. Similar behaviour is also observed for other Re values. The pressure drop decreased steadily along the channel, and a final value of 3 is attained at several half-channel widths downstream. Nevertheless, the steady pressure drop is reached much earlier than the complete flow and orientation development.

7. Conclusions

The influence of Reynolds number, Re, and a nondimensional suspension parameter, C, on the planar channel entry flow of slender fiber suspensions is

studied numerically. At the inlet, a uniform velocity profile and a random fiber orientation distribution are introduced. Near the entrance, large velocity and orientation gradients are observed for different values of the suspension parameter C and Re. A detailed study of the inlet regions shows that the inlet length increases significantly when fibers are added to the flow, and for high C values, the effect of Reynolds number becomes insignificant. In addition, when enough fibers are added, the concavity in the velocity profile near the entrance is eliminated. In the downstream region, the parabolic velocity profile and almost perfect fiber alignment along the flow direction are obtained after a rather long channel entry, depending on the values of C and Re. However, the steady pressure drop is achieved before the orientation and the flow fields are fully developed.

The accuracy of differential orientation evolution equations with quadratic closure approximations in predicting the flow kinematics and the orientation field is also analyzed. Numerically stable and convergent numerical results are not obtained for C values larger than 30. Moreover, by using orientation evaluation equations, the fiber alignment is predicted to be much quicker in channel flows such that the channel entry length is calculated to be much shorter than the actual length.

Appendix: Analytical solutions of planar orientation tensors in simple shear and planar elongational flows

For planar orientation states, the integrals given in Eqs. (25) and (26) can be analytically evaluated for an arbitrary homogeneous flow. The general analytical expressions for the second- and fourth-order tensor components are provided by Altan and Tang [40]. In deriving these equations, the analytical expression for the orientation distribution function given in Eq. (38) is utilized.

(1) For simple shear flow, the fourth-order orientation tensor components can be expressed as

$$
\begin{aligned}
S_{1111} &= \frac{4 + 5d_1 + 2d_1^2 + d_3}{2[(d_1 + d_3) + 2]^2}, \\
S_{1112} &= -\frac{(1 + d_1)d_2}{2[(d_1 + d_3) + 2]^2}, \\
S_{1122} &= \frac{d_1 + 2d_1 d_3 + d_3}{2[(d_1 + d_3) + 2]^2}, \\
S_{1222} &= -\frac{(1 + d_3)d_2}{2[(d_1 + d_3) + 2]^2}, \\
S_{2222} &= \frac{4 + d_1 + 5d_3 + 2d_3^2}{2[(d_1 + d_3) + 2]^2},
\end{aligned}
\tag{A1}
$$

where

$$d_1 = 1 + \frac{2\lambda}{1-\lambda}\sin^2 \omega t,$$
$$d_2 = -\frac{2\lambda}{\sqrt{1-\lambda^2}}\sin 2\omega t,$$
$$d_3 = 1 - \frac{2\lambda}{1+\lambda}\sin^2 \omega t, \tag{A2}$$
$$\omega = \left|\frac{1}{2}\frac{du}{dy}\sqrt{1-\lambda^2}\right|,$$

and, du/dy and t are shear rate and time, respectively. The parameter λ depends on the particle aspect ratio as given in Eq. (23).

(2) For planar elongation flow, the fourth-order orientation tensor components become

$$S_{1111} = \frac{2d_1^2 - 3d_1 + d_3}{2(d_3 - d_1)^2},$$
$$S_{1112} = 0,$$
$$S_{1122} = \frac{d_1 + d_3 - 2d_1 d_3}{2(d_3 - d_1)^2}, \tag{A3}$$
$$S_{1222} = 0,$$
$$S_{2222} = \frac{d_1 - 3d_3 + 2d_3^2}{2(d_3 - d_1)^2},$$

where

$$d_1 = e^{2\lambda\epsilon},$$
$$d_2 = 0,$$
$$d_3 = e^{-2\lambda\epsilon}, \tag{A4}$$
$$\epsilon = \left|\frac{du}{dx}\right| t,$$

and ϵ is the total elongation.

References

[1] H. Schlichting, Boundary Layer Theory, 4th edn., McGraw-Hill, New York, 1960, p. 168.
[2] M. Van Dyke, Entry flow in a channel, J. Fluid Mech., 44(4) (1970) 813–823.
[3] Y.L. Wang and P.A. Longwell, Laminar flow in the inlet section of parallel plates, AIChE J., 10(3) (1964) 323–329.
[4] B. Atkinson, M.P. Brocklebank, C.C.H. Card and J.M. Smith, Low Reynolds number developing flows, AIChE J., 15(4) (1969) 548–553.

[5] M. Tachibana, N. Kawabata and H. Genno, Steady laminar flow of power-law fluids in the inlet region of rectangular ducts, J. Rheol., 30(3) (1986) 517–538.
[6] R.C. Gupta, Laminar two-dimensional entrance region flow of power-law fluids, Acta Mech., 67 (1987) 129–137.
[7] S.S. Chen, L.T. Fan and C.L. Hwang, Entrance region flow of the bingham fluid in a circular pipe, AIChE J., 16(2) (1970) 293–299.
[8] A.B. Metzner and J.L. White, Flow behaviour of viscoelastic fluids in the inlet region of a channel, AIChE J., 11(6) (1965) 989–995.
[9] E. Bilgen, Behaviour of dilute polymer solutions in the inlet region of a pipe, J. Appl. Mech., 40(2) (1973) 381–387.
[10] D.V. Boger, Viscoelastic flows through contractions, Annu. Rev. Fluid Mech., 19 (1987) 157–182.
[11] J.G. Evans, The effect of the non-Newtonian properties of a suspension of rod-like particles on flow fields, in J.F. Hutton, J.R.A. Pearson and K. Walters (Eds.), Theoretical Rheology, Applied Science Publishers, London, 1975 pp. 224–232.
[12] T.C. Papanastasiou and A.N. Alexandrou, Isothermal extrusion of non-dilute fiber suspensions, J. Non-Newtonian Fluid Mech., 25 (1987) 313–328.
[13] S.M. Dinh and R.C. Armstrong, A rheological equation of state for semiconcentrated fiber suspensions, J. Rheol., 28(3) (1984) 207–227.
[14] G.G. Lipscomb, M.M. Denn, D.U. Hur and D.V. Boger, The flow of fiber suspensions in complex geometries, J. Non-Newtonian Fluid Mech., 26 (1988) 297–325.
[15] G.K. Batchelor, The stress system in a suspension of force-free particles, J. Fluid Mech., 41(3) (1970) 545–570.
[16] J.G. Evans, The flow of a suspension of force-free rigid rods in a Newtonian fluid, Ph. D. Dissertation, University of Cambridge, 1975.
[17] E.J. Hinch and L.G. Leal, Constitutive equations in suspension mechanics. Part 1. General formulation, J. Fluid Mech., 71(3) (1975) 481–495.
[18] E.J. Hinch and L.G. Leal, Constitutive equations in suspension mechanics. Part 2. Approximate forms for a suspension of rigid particles affected by Brownian rotations, J. Fluid Mech., 76(1) (1976) 187–208.
[19] J.L. Ericksen, Transversely isotropic fluids, Kollid-Z., 173 (1960) 117–122.
[20] K. Chiba, K. Nakamura and D.V. Boger, A numerical solution for the flow of dilute fiber suspensions through an axisymmetric contraction, J. Non-Newtonian Fluid Mech., 35 (1990) 1–14.
[21] J. Rosenberg, M.M. Denn and R. Keunings, Simulations of non-recirculating flows of dilute fiber suspensions, J. Non-Newtonian Fluid Mech., 37 (1990) 317–345.
[22] N. Phan-Thien and A.L. Graham, A new constitutive model for fibre suspensions: Flow past a sphere, Rheol. Acta, 30 (1991) 44–57.
[23] M.C. Altan, S.I. Güçeri and R.B. Pipes, Anisotropic channel flow of fiber suspensions, J. Non-Newtonian Fluid Mech., 42 (1992) 65–83.
[24] R.A. Keiller and E.J. Hinch, Corner flow of a suspension of rigid rods, J. Non-Newtonian Fluid Mech., 40 (1991) 323–335.
[25] R.A. Keiller, J.M. Rallison and J.G. Evans, Sink flows of a suspension of rigid rods: The failure of a similarity solution, J. Non-Newtonian Fluid Mech., 42 (1992) 249–266.
[26] J.M. Rallison and R.A. Keiller, Sink flows of a suspension of rigid rods: Part 2. Lubrication theory, J. Non-Newtonian Fluid Mech., 48 (1993) 237–259.
[27] M.C. Altan, A review of fiber-reinforced injection molding: Flow kinematics and particle orientation, J. Thermoplastic Compos. Mater., 3(4) (1990) 275–313.
[28] C.L. Tucker III, Flow regimes for fiber suspensions in narrow gaps, J. Non-Newtonian Fluid Mech., 39 (1991) 239–268.
[29] E.S.G. Shaqfeh and G.H. Fredrickson, The hydrodynamic stress in a suspension of rods. Phys. Fluids A, 2(1) (1990) 7–24.
[30] M.A. Bibbo, S.M. Dinh and R.C. Armstrong, Shear flow properties of semi-concentrated fiber suspensions, J. Rheol., 29 (1985) 905–929.
[31] G. Ausias, J.F. Agassant, M. Vincent, P.G. Lafleur, P.A. Lavoie and P.J. Carreau, Rheology of short glass fiber reinforced polypropylene, J. Rheol., 36(4) (1992) 525–542.

[32] G.B. Jeffery, The motion of ellipsoidal particles immersed in a viscous fluid, Proc. R. Soc. London, Ser.A, 102, (1922) 161–179.
[33] G.L. Hand, A theory of anisotropic fluids, J. Fluid Mech., 13 (1962) 33–46.
[34] M. Doi, Molecular dynamics and rheological properties of concentrated solutions of rodlike polymers in isotropic and liquid crystalline phases, J. Polym. Sci., Polym. Phys. Ed., 19 (1981) 229–243.
[35] M.C. Altan, S. Subbiah, S.I. Güçeri and R.B. Pipes, Numerical prediction of three-dimensional fiber orientation in Hele–Shaw flows. Polym. Eng. Sci., 30(14) (1990) 848–859.
[36] S.G. Advani and C.L. Tucker III, The use of tensors to describe and predict fiber orientation in short fiber composites, J. Rheol., 31(8) (1987) 751–784.
[37] S.G. Advani and C.L. Tucker III, Closure approximations for three-dimensional structure tensors, J. Rheol., 34(3) (1990) 367–386.
[38] M.C. Altan, S.G. Advani, S.I. Güçeri and R.B. Pipes, On the description of the orientation state for fiber suspensions in homogeneous flows, J. Rheol., 33(7) (1989) 1129–1155.
[39] P.L. Maffettone and G. Marrucci, A two-dimensional approach to the constitutive equation of nematic polymers, J. Non-Newtonian Fluid Mech., 38 (1990) 273–288.
[40] M.C. Altan and L. Tang, Orientation tensors in simple flows of dilute suspension of non-Brownian rigid ellipsoids; Comparison of analytical and approximate solutions, Rheol. Acta, 32(3) (1993) 227–244.
[41] S.J. Lee, Numerical study on three-dimensional flow of fiber suspensions, Ph. D. Dissertation, Seoul National University, 1992.
[42] A.J. Szeri and L.G. Leal, A new computational method for the solution of flow problems of microstructured fluids. Part 1. Theory, J. Fluid Mech., 242 (1992) 549–576.
[43] A.J. Szeri and L.G. Leal, A new computational method for the solution of flow problems of microstructured fluids. Part 2. Inhomogeneous shear flow of a suspension, J. Fluid Mech., 262 (1994) 171–204.
[44] S. Akbar and M.C. Altan, On the solution of fiber orientation in two-dimensional homogeneous flows, Polym. Eng. Sci., 32(12) (1992) 810–822.
[45] A.J. Szeri, Pattern formation in recirculating flows of suspensions of orientable particles, Philos. Trans. R. Soc. London Ser.A, 345 (1993) 477–506.